0026-895X/86/040388-10$0.00/0

MOLECULAR PHARMACOLOGY, 30:388-397

Rat Heart Anthracycline-Binding Polypeptides Identified by Photoaffinity Labeling

RONALD L. FELSTED, CONSTANCE J. GLOVER, RONALD E. CLAWSON,[1] and STEVEN D. AVERBUCH[2]

Laboratory of Biological Chemistry, Developmental Therapeutics Program, Division of Cancer Treatment, National Cancer Institute, National Institutes of Health, Bethesda, Maryland 20892

Received March 6, 1986; Accepted July 9, 1986

SUMMARY

A radioactive, photoactive anthracycline analogue, *N*-(*p*-azido-[3,5-^{3}H]benzoyl)-daunorubicin (^{3}H-NAB-daunorubicin), was synthesized and characterized by UV-visible absorption and infrared analyses. ^{3}H-NAB-daunorubicin photoaffinity labeling of rat heart homogenates resulted in the identification of two prominently radiolabeled anthracycline-binding polypeptides of 18.3 and 31.2 kDa. Photoaffinity labeling with photoactive doxorubicin (Adriamycin), carminomycin, and nonanthracycline model compounds resulted in a clear structural dependence for binding to the 18.3- and 31.2-kDa species. In the presence of daunorubicin or *N*-substituted daunorubicin analogues, ^{3}H-NAB-daunorubicin photolabeling of the 18.3-kDa polypeptide was inhibited. Photolabeling was dependent on time of UV light exposure and protein concentration and was unaffected by the presence of nitrene scavengers. The 18.3-kDa polypeptide photolabeling was saturable and reversed by >90% in the presence of a 16-fold molar excess of nonradioactive analogue. Photolabeling of heart subcellular fractions demonstrates that both the 18.3- and 31.2-kDa polypeptides were localized to the inner mitochondrial membrane. Since the anthracyclines are known to have several effects on heart mitochondrial function, the identification of specific polypeptide acceptors using photoactive anthracycline analogues may elucidate biochemical mechanisms of anthracycline cellular activity.

Anthracycline antibiotic affinity for DNA is thought to account for a number of drug-induced nuclear events which result in anthracycline cytotoxic activity. Although these nuclear effects are undoubtedly important, recent additional hypotheses to explain anthracycline activity have been forwarded based on observations that these compounds are capable of interacting with and affecting the functions of multiple subcellular organelles and macromolecular targets (1–7). This multiplicity of interactions is not unexpected since the anthracyclines are complex molecules with amphipathic and amphoteric properties which lead to their association with a variety of cellular components such as nucleic acids, mucopolysaccharides, lipids, and proteins (8–21). However, few examples of specific anthracycline antibiotic-protein associations have been described because of the practical limitation of measuring unique drug interactions in the presence of extensive nonspecific adsorption to soluble and particulate constituents as well as to experimental apparatus. In previous studies, the demonstration of apparent specific drug-protein interactions required an *a priori* assumption of drug involvement in a particular biochemical process and/or the availability of purified proteins for equilibrium binding measurements under optimum conditions (11, 15, 18–20, 22).

Many of the difficulties in the identification of anthracycline-binding proteins can be circumvented by photoaffinity labeling. This approach can distinguish inconsequential nonspecific binding from specific anthracycline binding under conditions where the relationship between drug distribution among subcellular and soluble components and drug-associated biochemical activities is preserved. Under these conditions, photolabeling should reflect drug-protein interactions which have biological importance (23, 24).

The photoaffinity labeling technique was recently used to identify cell surface protein(s) as the possible site(s) of daunorubicin interaction(s) in Sarcoma 180 cells (25). However, in that study only general anthracycline protein binding was demonstrated, and the functional significance of these inter-

[1] Present address: U. S. Army Medical R and D Command, att. SGRD-PLE-Dr. Clawson, Fort Detrick, Frederick, MD 21701.

[2] Present address: Division of Clinical Pharmacology, Department of Pharmacology, Uniformed Services University of the Health Sciences, Bethesda, MD 20814-4799.

ABBREVIATIONS: NAB-daunorubicin, *N*-(*p*-azidobenzoyl)-daunorubicin, NAB-Adriamycin, *N*-(*p*-azidobenzoyl)-Adriamycin; NAB-carminomycin, *N*-(*p*-azidobenzoyl)-carminomycin; NAB-daunosamine, *N*-(*p*-azidobenzoyl)-daunosamine; NAB-ethanolamine, *N*-(*p*-azidobenzoyl)-ethanolamine; NAB-daunorubicinol, *N*-(*p*-azidobenzoyl)-daunorubicinol; ^{3}H-NAB-daunorubicin, -Adriamycin, -carminomycin, -ethanolamine, or -daunosamine, *N*-(*p*-azido-[3,5-^{3}H]benzoyl)-daunorubicin, -Adriamycin, -carminomycin, -ethanolamine, or -daunosamine; SDS, sodium dodecyl sulfate; PAGE, polyacrylamide gel electrophoresis; TLC, thin layer chromatography; HPLC, high performance liquid chromatography; EDTA, ethylenediaminetetraacetate; EGTA, ethylene glycol bis(β-aminoethyl ether)-*N,N,N′,N′*-tetraacetic acid; MOPES, 3-[*N*-morpholino]propanesulfonate:

actions was not known. In the present report, we describe the synthesis of pharmacologically active (26), radioactive, photoactive anthracycline analogues and use them to identify specific anthracycline-binding polypeptides in rat heart. Since the well known cardiotoxic effects of anthracyclines (27) are most likely determined by these primary cellular interactions, the identification of unique anthracycline acceptors should assist in clarifying the biochemical mechanisms of anthracycline antibiotic toxicity.

Experimental Procedures

Materials

Daunorubicin-HCl, doxorubicin (Adriamycin)-HCl, carminomycin-HCl, daunosamine-HCl, *N,N'*-dibenzyldaunorubicin, and *N*-acetyldaunorubicin were obtained from the Drug Synthesis and Chemistry Branch of the National Cancer Institute, Bethesda, MD. Daunorubicin and Adriamycin were further purified by silica gel chromatography (28). NAB-Daunorubicin, NAB-Adriamycin, and NAB-carminomycin were synthesized as described below. Daunorubicinol and NAB-daunorubicinol were prepared enzymatically from daunorubicin and NAB-daunorubicin, respectively, with 0.138 mg/ml of rat liver daunorubicin reductase in 10 mM Tris-HCl buffer, pH 8.5, and supplemented with 5 mM NADPH (P & L Biochemicals, Milwaukee, WI) (29). 7-Deoxydaunorubicin aglycone and 7-deoxydaunorubicinol aglycone were prepared from daunorubicin and daunorubicinol, respectively, by anaerobic treatment with 3–4-fold molar excess of sodium dithionite in 0.1 M $NaHCO_3$ (20). *N*-(*p*-Aminobenzoyl)-daunorubicin was prepared from NAB-daunorubicin with 10 mM dithiothreitol in 0.1 M Tris-HCl buffer, pH 8.4, as previously described (30) and purified by silica gel chromatography (28).

Syntheses

NAB-daunorubicin. *N*-Hydroxysuccinimidyl-4-azidobenzoate (10 μmol) (Pierce Chemical Co., Rockford, IL), K_2CO_3 (20 μmol), and daunorubicin-HCl (5 μmol) in 1 ml of 5% methanol in chloroform were heated at 40° for 12–15 hr. The solvent was evaporated, and the dry residue was suspended in 1 ml of deionized water and incubated an additional 15 min. This heated mixture was adjusted to pH 6.0 with 1 M potassium phosphate buffer and extracted with 0.5 ml of hexane; then, the hexane layer was removed and discarded. The product, NAB-daunorubicin, was recovered by 8–10 sequential extractions with 0.5-ml aliquots of diethyl ether. The ether extracts were pooled, evaporated to 1–2 ml, and applied to a column (0.5 × 7 cm) of silica gel equilibrated in chloroform. After washing with 2–3 ml of ether, the product was eluted from the column with 5% methanol in chloroform. A yield of about 71% was obtained. The product gave a single fluorescent spot on silica gel TLC (E. Merck, Darmstadt, West Germany) and no other UV-absorbing spots were seen on silica gel TLC with fluorescent indicator (E. Merck) [solvent I (chloroform:methanol:water, 80:20:3) $R_f = 0.71$; solvent II (choloroform:methanol:acetic acid, 100:2:2.5), $R_f = 0.27$]. Reverse phase HPLC indicated a single product accounting for 98% of the fluorescence eluted. The final product exhibited an IR spectrum with a strong azide resonance at 2120 cm^{-1}. The fluorescence emission spectrum was identical with that of daunorubicin (data not shown).

NAB-Adriamycin and NAB-carminomycin. NAB-Adriamycin and NAB-carminomycin were synthesized from *N*-hydroxysuccinimidyl-4-azidobenzoate and Adriamycin-HCl or carminomycin-HCl and purified as described above, except for the following changes. The products were recovered by extracting with ethyl acetate (NAB-Adriamycin) or ether (NAB-carminomycin) and purified by silica gel chromatography. After washing the silica gel column with ether, the products were eluted with 2% methanol in chloroform. The products gave single fluorescent spots on silica gel TLC and no other UV-absorbing spots were seen on silica gel containing fluorescent indicator. (solvent I: $R_f = 0.68$ (NAB-Adriamycin), $R_f = 0.78$ (NAB-carminomycin); solvent II: $R_f = 0.086$ (NAB-Adriamycin), $R_f = 0.29$ (NAB-carminomycin). A single peak accounting for >99% of eluted fluorescence was detected by reverse phase HPLC for both compounds. The final products exhibited IR spectra with strong azide resonance at 2100 cm^{-1}.

^{3}H-NAB-daunorubicin, ^{3}H-NAB-Adriamycin, and ^{3}H-NAB-carminomycin. *N*-Hydroxysuccinimidyl-4-azido-[3,5-^{3}H]-benzoate (1.15–4.6 nmol, 36.8–50.6 Ci/mmol, New England Nuclear, Boston, MA), anhydrous K_2CO_3 (10 μmol), and daunorubicin, Adriamycin, or carminomycin (0.5 μmol) in 0.5 ml of 10% methanol in chloroform were heated at 40° for 12–15 hr. The product was extracted and purified as described above for the nonradioactive compounds. Identity and purity were confirmed by silica gel TLC in solvents I and II.

NAB-ethanolamine. *N*-Hydroxysuccinimidyl-4-azidobenzoate (0.2 mmol) and ethanolamine (1.2 mmol) were incubated in 2 ml of chloroform for 1 hr at 40°. The reaction solvent was evaporated and the dry residue was extracted with a mixture of methanol:chloroform:10% Na_2CO_3 (1:1:1, v/v/v). The lower chloroform layer was recovered and the extraction was continued with additional chloroform aliquots until all UV-absorbing material was recovered from the upper phase. The combined chloroform extracts were evaporated and the residue was suspended in 1 ml of chloroform and repeatedly extracted with 1-ml aliquots of deionized water until all ninhydrin-positive material was removed from the chloroform layer. The product from the final chloroform layer was recovered by evaporation, dissolved in deionized water, and lyophilized (80% yield). A single UV-absorbing spot was seen on silica gel TLC (solvent II, $R_f = 0.18$) and by reverse phase silica gel TLC (Analtech, Inc., Newark, DE) [solvent III (methanol:H_2O; 50:50), $R_f = 0.68$]. The IR spectra exhibited a strong azide resonance at 2120 cm^{-1}. The direct electrical impact mass spectrum was: M^+ 206, *m/z* 178, 161, 146, and 118.

^{3}H-NAB-ethanolamine. *N*-Hydroxysuccinimidyl-4-azido-[3,5-^{3}H]-benzoate (1 nmol, 50.6 Ci/mmol) and ethanolamine (0.15 mmol) were incubated in 0.050 ml of isopropanol at 40° for 2 hr and extracted as described for NAB-ethanolamine. The chloroform solvent was evaporated, the residue was suspended in chloroform, and the insoluble material was discarded. The product was recovered from the chloroform by evaporation. The identity and purity of the product were confirmed by silica gel and reverse phase silica gel TLC in solvents II and III, respectively.

NAB-daunosamine. Daunosamine-HCl (120 μmol), anhydrous K_2CO_3 (150 μmol), and *N*-hydroxysuccinimidyl-4-azidobenzoate (240 μmol) were dissolved in 1.5 ml of distilled dimethylformamide and heated at 40° for 12–15 hr. The solvent was evaporated and the residue extracted as described for NAB-ethanolamine. The combined chloroform extracts were dried and the residue was dissolved in a minimal volume of methanol, applied to the preadsorbent strip of a tapered preparative silica gel TLC (with fluorescent indicator) (Analtech, Inc.) (prewashed with solvent I), and developed in solvent I. The UV-absorbing components were located as quenching regions on guide strips with UV light. The slowest migrating major UV-absorbing species was recovered by extracting the silica gel with 10% methanol in chloroform. The product was recovered, dissolved in deionized water, and lyophilized (20% yield). A single UV absorbing spot was detected on silica gel and reverse phase silica gel TLC developed in solvent I ($R_f = 0.43$) and solvent III ($R_f = 0.67$), respectively. The IR spectrum exhibited a strong azide resonance at 2120 cm^{-1}. The fast atom bombardment mass spectrum was: M + H + glycerol 385, M + Na 315, M + H 293, and M + H − HOH 275.

^{3}H-NAB-daunosamine. Daunosamine-HCl (5.3 μmol), *N*-hydroxysuccinimidyl-4-azido-[3,5-^{3}H]-benzoate (1 nmol, 50.6 Ci/mmol) and anhydrous K_2CO_3 were incubated in dimethylformamide and purified as described for NAB-daunosamine. Product identity and purity (97% of total radioactivity) were confirmed by silica gel TLC (solvent I).

Tissue homogenate and supernatant fractions. Sprague-Dawley rats (200–300 g) were killed by cervical dislocation and the organs (i.e., heart, liver, kidney, lung, brain, intestine, and skeletal muscle) were

removed and homogenized in 10 volumes (w/v) of 0.05 M potassium phosphate buffer, pH 7.4, for 1 min with a model PCU Polytron homogenizer with a PT-10-ST probe (Brinkmann Instruments, Westbury, NY) operated at 50% maximum power. This and all subsequent operations were at 0–5°. The tissue homogenates were obtained after filtering through one layer of cheese cloth. Tissue supernatant fractions were prepared by centrifuging tissue homogenates at 100,000 × *g* for 60 min at 0–5° (model L5-50, Beckman Instruments, Palo Alto, CA). Studies were carried out with either fresh tissue homogenates and supernatant fractions or with homogenates and supernatant fractions stored in small aliquots in liquid nitrogen and thawed only once.

Photoactivation conditions. Unless otherwise stated, the standard photolabeling mixture included: 59–64 nM ^{3}H-NAB-daunorubicin, ^{3}H-NAB-Adriamycin, ^{3}H-NAB-carminomycin, ^{3}H-NAB-daunosamine, or ^{3}H-NAB-ethanolamine, 4% dimethyl sulfoxide, 40 mM potassium phosphate buffer, pH 7.0, and 1.6–2 mg/ml of tissue homogenate or supernatant fraction protein in a final volume of 0.050 ml. Mixtures were preincubated for 15 min at 25°. Photolabeling was accomplished by irradiating for 10–20 min with a UV light equipped with two 15-W self-filtering 302-nm lamps (model xx-15, Ultra-Violet Products, Inc., San Gabriel, CA) suspended 3.4 cm above the photolabeling mixtures which were in polyvinylchloride V-microtiter wells (Dynatech Laboratories, Inc., Alexandria, VA) in a 25° water bath. Irradiated samples were either frozen at −15° or immediately processed for SDS-PAGE.

The radioactivity of photolabeled components was quantitated in triplicate by summing the dpm in each 1-mm gel slice across the radioactive peak, subtracting the average baseline radioactivity, and expressing the result as a mean ± standard deviation.

Macromolecular composition of anthracycline-binding components. Heart (85 μg of protein) homogenates were photolabeled with ^{3}H-NAB-daunorubicin under standard irradiation conditions and then incubated either with 1 mg/ml of proteinase K (E. Merck) in 2% SDS, 2.5 mM EDTA, and 50 mM glycine-NaOH buffer, pH 10.1 (final volume 0.1 ml) for 1 hr at 37°, or with 0.214 mg/ml of DNase (2182 units/mg; Millipore Corp., Bedford, MA) and 0.107 mg/ml of RNase (5331 units/mg; Millipore) in 4.5 mM $MgCl_2$, 18 mM $CaCl_2$, and 2 mM potassium phosphate buffer, pH 7.0 (final volume 0.1 ml) for 5 min at 37°. The incubation mixtures were prepared for SDS-PAGE as described below. Macromolecular lipids were extracted (three times) from photolabeled heart homogenate with 5 volumes of chloroform:methanol (2:1; v/v) (16). The combined extracts were mixed with chloroform:methanol:water (0.5:4:4, v/v/v) and, after overnight partitioning at 4°, the lower chloroform layer was removed. The upper aqueous layer was washed with another 0.5 volume of fresh chloroform, and both chloroform layers were combined and evaporated with a stream of N_2. The residue was prepared for SDS-PAGE as described below.

Subcellular fractionation. Purified mitochondria were prepared by homogenizing minced rat heart with a Potter-Elvehjem tissue homogenizer (31) in 4 ml of 0.225 M mannitol, 0.075 M sucrose, 10 mM EGTA, and 5 mM MOPES (pH 7.4) containing 0.40 mg of Nagarse (protease type VII, Sigma Chemical Co., St. Louis, MO) per g of heart (32). Immediately after homogenization, the tissue homogenate was diluted to 5% in mannitol/sucrose/EGTA/MOPES buffer containing 0.2% bovine albumin. The diluted homogenate was centrifuged at 480 × *g* for 10 min and the mitochondria in the supernatant fraction were recovered by centrifuging at 3020 × *g* for 10 min (33). After removal of the fluffy coat, the final mitochondrial pellet was suspended in 150 mM KCl and 10 mM MOPES, pH 7.4. The mitochondrial fractions were analyzed by the following enzyme assays: cytochrome oxidase (34), succinate cytochrome *c* reductase (35), *N*-acetyl-β-glucosaminidase (36), NADPH cytochrome *c* reductase (35), 5′-nucleotidase (37), and lactate dehydrogenase (38).

Submitochondrial fractionation. The mitochondria used for submitochondrial fractionation were isolated from rat heart by the procedure of Sorbahl *et al.* (39). Mitochondrial outer membrane, intermembrane space, inner membrane, and matrix fractions were isolated from digitonin-treated mitochondria as previously described (40). The following enzyme assays were performed on each fraction: monoamine oxidase (outer membrane) (41), adenylate kinase (intermembrane space) (42), cytochrome oxidase (inner membrane (34), and glutamate dehydrogenase (matrix) (42). The relative specific activities and histogram analysis were determined according to the method of Beaufay and Amar-Costesec (43).

SDS-PAGE. Photolabeled mixtures were prepared for SDS-PAGE by mixing with an equal volume of SDS-sample buffer (4% SDS, 8 M urea, 0.1 M dithiothreitol, 20% glycerol, 0.04% bromophenyl blue, and 0.08 M Tris-HCl buffer, pH 6.8), and the suspensions were transferred to 0.5-ml microcentrifuge tubes and heated for 5 min at 100° in a heating block. After cooling on ice, the heat-treated mixtures were sonicated for 5 sec (continuous, 50% maximum output with a microprobe; model W-225R, Ultrasonics, Inc., Plainview, NY), and again cooled on ice, and aliquots (0.075 ml) were applied to separate slots of a polyacrylamide slab gel.

SDS-PAGE was run with a slab gel apparatus (model 220, Bio-Rad Laboratories, Richmond, CA) on 1.5-mm-thick gels made with a 10- or 15-slot sample comb. Electrophoresis was carried out as previously described (44) using a linear polyacrylamide gradient: 9.7% acrylamide, 0.26% bisacrylamide, and 10% gylcerol to 16.6% acrylamide, 0.44% bisacrylamide, and 17% glycerol. Electrophoresis was performed at 8 mamp/gel for 16 hr. The gel was fixed and stained in 0.25% Coomassie brilliant blue in 45% methanol and 10% acetic acid and destained by diffusion against 20% methanol and 10% acetic acid. The lanes of stained polypeptides corresponding to each sample slot were cut from the destained slab gel and cross-sectioned into 1.0-mm slices. Each slice was incubated with 0.15 ml of 30% H_2O_2 in closed scintillation vials for 2 hr at 70–80° or until the gel slices were solubilized. They were then mixed with aqueous counting scintillant, NCS (Amersham Corp., Arlington Heights, IL) and measured in a scintillation counter (model Prias, Packard Instrument Co., Downers Grove, IL). The electrophoretic migration of radioactive macromolecules was compared to low molecular weight polypeptide standards (Bio-Rad).

Analytical Methods

Analysis of radioactive compounds by TLC was accomplished by scraping silica gel from the plate every 0.5 cm, suspending the silica gel in scintillation cocktail, and counting in a liquid scintillation counter.

The UV-visible absorption spectra were determined on a diode array spectrophotometer (model 8450A, Hewlett-Packard Scientific Instruments Division, Palo Alto, CA). IR spectra were performed on a model 727B infrared spectrophotometer (Perkin-Elmer). Direct electrical impact mass spectra were obtained on a Ribermag gas chromatography/mass spectrometer system (Mass range 0–1500 amu, model R10-10-C, RDS Nermag, Inc., Houston, TX). The sample was dissolved in chloroform, an aliquot was deposited on the direct electrical impact probe, and the solvent was evaporated with a stream of N_2. Following insertion of the direct electrical impact probe, the current in the direct electrical impact filament was linearly increased from 20 to 400 mamp at 7 mamp/sec to volatilize the sample. Fast atom bombardment mass spectra were obtained on a V.G. Analytical (Altrincham, U.K.) 7070E double focusing mass spectrometer fitted with an Ion-Tech (Teddington, U.K.) saddlefield gun, using xenon. Samples were loaded onto the probe by suspension in 1 μl of glycerol.

HPLC analysis was accomplished on a μBondapak phenyl column (3.9 mm × 30 cm) (Waters Associates, Milford, MA) fitted with two pumps (model 100A, Beckman Instruments) and a fluorometer (model 121, Gilson Medical Electronics, Middleton, WI) containing activation (480 nm) and emission (560 nm) filters. Analytical reverse phase separations were achieved with a linear gradient from 15 to 50% tetrahydrofuran in 0.1 g/100 ml ammonium formate buffer, pH 4.0, in 10 min at a flow rate of 2 ml/min, described previously (45). This was followed by a 5-min isocratic elution with 50% tetrahydrofuran in the same buffer at the end of the gradient. With this system, daunorubicinol, 7-deoxydaunorubicinol aglycone, daunorubicin, 7-deoxydaunorubicin aglycone, NAB-Adriamycin, NAB-daunorubicinol, NAB-dauno-

rubicin, and NAB-carminomycin had retention times of 8.6, 9.8, 10.1, 11.7, 12.4, 12.5, 13.7, and 16.1 min, respectively.

Tissue homogenates and supernatant fractions were treated with 1 M NaOH for 30 min at room temperature and soluble protein was determined by comparison to a bovine albumin standard curve (46). Fluorography was performed by the procedure of Bonner and Laskey (47).

Results

Synthesis and characterization of photoactive anthracycline analogues. The photoactive anthracycline analogues, NAB-daunorubicin, NAB-Adriamycin, and NAB-carminomycin, were prepared by *N*-azidobenzoylation of daunorubicin, Adriamycin, and carminomycin, respectively, with *N*-hydroxysuccinimidyl-4-azido-benzoate. Similar reactions with daunosamine and ethanolamine yielded photoactive model compounds lacking either the anthracyclinone ring (NAB-daunosamine) or both the anthracyclinone ring and the amino sugar (NAB-ethanolamine), respectively. The UV-visible absorption spectrum of NAB-daunorubicin was a composite of the spectra of its component chromophores, i.e., the *p*-azidobenzoyl group (λ_{max} 270 nm) and the daunomycinone ring (λ_{max} 470, 485, 560 nm). Upon UV irradiation, the *p*-azidobenzoyl moiety was photoactivated with concomitant loss in UV absorption yielding a spectrum very similar to that of native daunorubicin (Fig. 1A). Similar results were obtained for the NAB-Adriamycin and NAB-carminomycin analogues. The spectra of NAB-daunosamine and NAB-ethanolamine were identical to each other and were entirely accounted for by the absorption of the *p*-azidobenzoyl chromophore. Upon UV irradiation, this absorption was substantially reduced (Fig. 1B). The photoactivation of standard photolabeling mixtures in the absence of added protein (up to 1.39 μM NAB-daunorubicin) showed a first order reduction of 270 nm of NAB-daunorubicin absorption with a $t_{½} = 79\ sec^{-1}$. A higher NAB-daunorubicin concentration (13.9 μM) resulted in a coincident photobleaching of the anthracyclinone ring absorption above 400 nm, probably due to photoactivated drug-drug cross-linking (data not shown) (48).

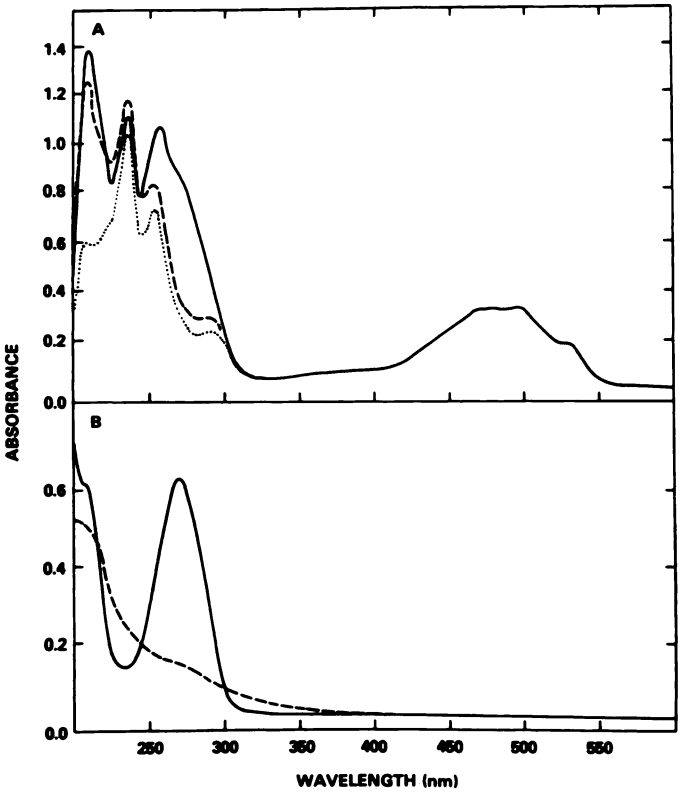

Fig. 1. UV-visible absorption spectra for: A, NAB-daunorubicin (—), NAB-daunorubicin after irradiation at a wavelength of 302 nm at a distance of 5 cm for 10 min (Experimental Procedures) (– – –), and daunorubicin (· · ·); and B, NAB-daunosamine (—) and NAB-daunosamine after irradiation at 302 nm at a distance of 5 cm for 10 min (– – –). The solvent was methanol.

Identification of rat tissue anthracycline binding components by photoaffinity labeling. The anthracycline photoaffinity labeling pattern of rat tissue was determined by UV irradiation of mixtures of ^{3}H-NAB-daunorubicin and tissue homogenate followed by SDS-PAGE. The radioactivity in 1-mm gel slices was compared to the migration of polypeptide molecular weight standards. The pattern of radioactive labeling of most major and minor photolabeled components was independent of the Coomassie brilliant blue-stained polypeptide patterns. As shown for rat heart (Fig. 2A), several major photolabeled components were superimposed on a baseline radioactivity of 2–4 times ambient background which was distributed throughout the gel. Overall, the heart homogenate 18.3- and 31.2-kDa species were the most prominently photolabeled components among all tissues examined. The 18.3-kDa species was also found in kidney and lung homogenates. The photolabeling pattern of the 100,000 × *g* clarified heart supernatant fraction was dramatically different from its homogenate profile (Fig. 2B). In particular, the supernatant fraction was characterized by the complete absence of the 18.3-kDa and the 31.2-kDa components. Thus, these major photolabeled heart species are localized exclusively in the 100,000 × *g* particulate fraction.

Because of the prominent photolabeling of these components and because of the important anthracycline effects on heart as

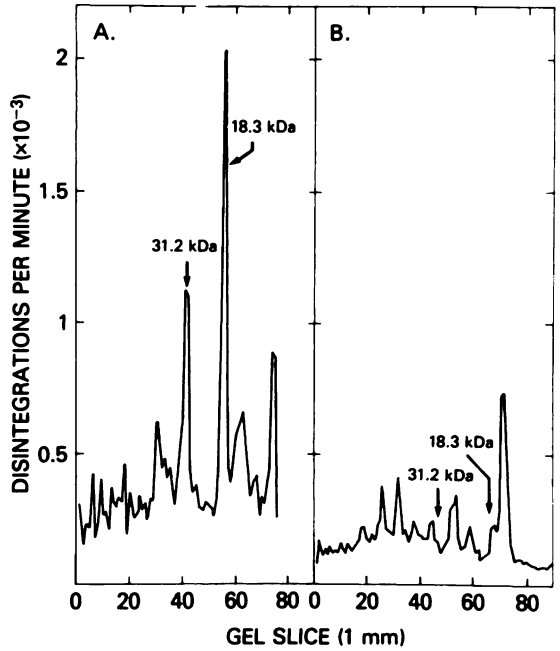

Fig. 2. SDS-PAGE profiles of rat heart homogenate (56 μg of protein) (A) and high speed supernatant fraction (B) following photolabeling with ^{3}H-NAB-daunorubicin. The *arrows* and associated *numbers* indicate (in kDa) the migration of radioactively labeled components relative to polypeptide molecular weight standards.

manifest by a severe dose-dependent cardiotoxicity (27), we further characterized the photolabeling of rat heart.

Subcellular localization of 18.3- and 31.2-kDa components. A probable mitochondrial localization of 18.3- and 31.2-kDa components was established by photolabeling purified heart mitochondria. Purified mitochondria exhibited a 1.46-fold increased 18.3-kDa component specific photolabeling relative to that of heart homogenate. This paralleled a 1.9-fold and a 2.4-fold increase in the specific activity of the mitochondrial marker enzymes, succinate cytochrome *c* reductase and cytochrome *c* oxidase, respectively, relative to a similar proteolytic enzyme-treated heart homogenate. Concomitantly, the specific activities of marker enzymes for other major subcellular organelles in the mitochondrial fraction were reduced. Substantial 31.2-kDa polypeptide also was recovered in the purified mitochondrial fraction, although relative specific photolabeling was not quantitated.

The mitochondrial localization of the 18.3- and 31.2-kDa polypeptides was confirmed and further characterized by quantitating the distribution of photolabeled components among submitochondrial fractions (Fig. 3). Greater than 95% of the 31.2-kDa specific photolabeling recovered was found in the inner mitochondrial membrane fraction, confirming an inner membrane localization (Fig. 3A). Sixty-eight per cent of the 18.3-kDa polypeptide also was found in the inner membrane fraction. However, a significant fraction (22%) of 18.3 kDa exhibited a higher specific photolabeling in the outer membrane fraction. Nevertheless, since the 18.3-kDa specific photolabeling does not parallel the distribution of the outer membrane marker enzyme, monoamine oxidase (Fig. 3C), and since substantial amounts of the inner membrane proteins may be released into the outer membrane fraction upon digitonin subfractionation of mitochondria (34) (Fig. 3E), the 18.3-kDa component most likely is localized with the inner mitochondrial membrane.

The relative abundance of radiolabeled 18.3- and 31.2-kDa polypeptides to total mitochondrial protein was evaluated by comparing the SDS-PAGE fluorograph of photolabeled rat heart mitochondria to the corresponding Coomassie blue-stained polypeptide pattern (Fig. 4). The 18.3-kDa radiolabeled component coelectrophoresed with a Coomassie blue-stained polypeptide doublet representing 2.6% of the total mitochondrial protein as determined by densitometry. In contrast, the 31.2-kDa component migrated near the trailing edge of a major polypeptide, accounting for 10–15% of the total mitochondrial protein stain. The slight shift of the 31.2-kDa mobility relative

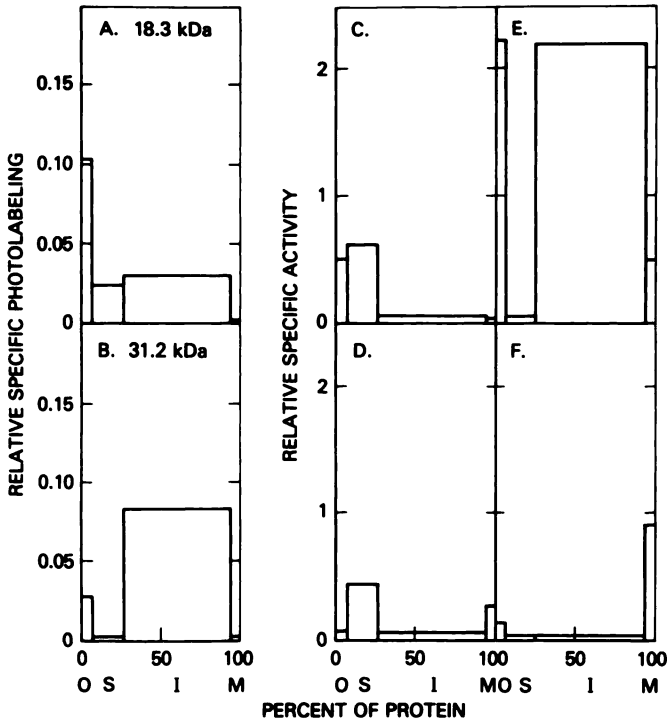

Fig. 3. The submitochondrial distribution of photolabeled 18.3-kDa and 31.2-kDa polypeptides. Digitonin-treated mitochondria were fractionated into outer membrane (*O*), intermembrane space (*S*), inner membrane (*I*), and matrix (*M*) fractions by differential centrifugation. These fractions are represented by *blocks* ordered according to the same sequence where they span a length on the *abscissa* proportional to their protein content. The *ordinate* gives the relative specific photolabeling (A and B) or relative specific activity (C–F) or content which is the percentage of polypeptide on enzyme activity recovered in each fraction over the percentage of protein of the same fraction. A, 18.3-kDa polypeptide; B, 31.2-kDa polypeptide; C, monoamine oxidase; D, adenylate kinase; E, cytochrome oxidase; and F, glutamate dehydrogenase.

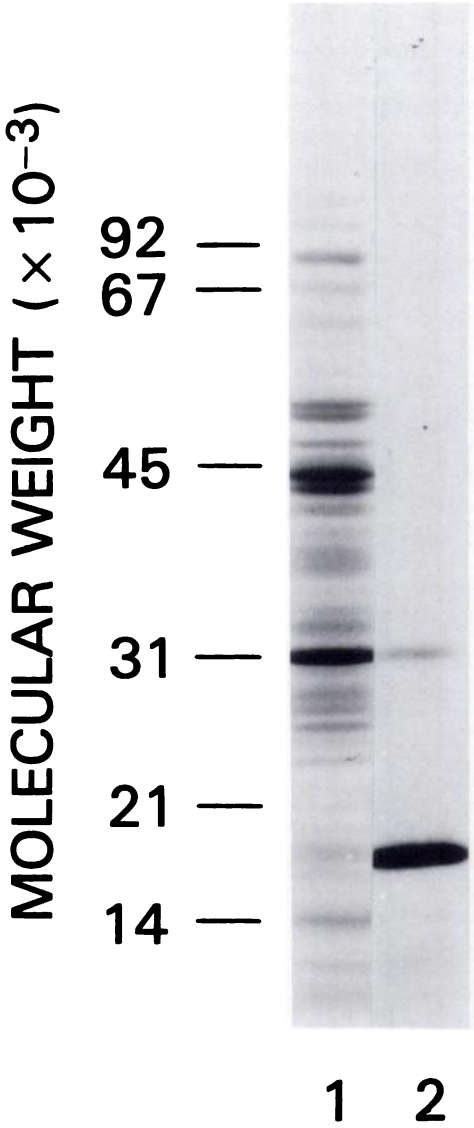

Fig. 4. SDS-PAGE of ^{3}H-NAB-daunorubicin photoaffinity-labeled rat heart mitochondria (100 μg of protein). The protein was stained with Coomassie blue (*lane 1*) and fluorographed (*lane 2*).

to the major mitochondrial polypeptide probably reflects an increase in the molecular mass of the 31.2-kDa polypeptide due to the covalent attachment of the photoactivated anthracycline analogue.

Molecular characterization of the photolabeled components. Specific hydrolytic enzymes were used to establish the protein nature of the photolabeled components. Treatment with DNase and RNase had no effect on either specific or baseline photolabeling. However, proteinase K treatment of photolabeled heart homogenate completely abolished all major labeled components as well as the baseline radioactivity. The denaturation of heart homogenates by heating at 100° for 10 min, just prior to photolabeling, completely eliminated the subsequent radiolabeling of 18.3- and 31.2-kDa components without significantly affecting the baseline radioactivity. The absence of 18.3- and 31.2-kDa photolabeling in heat-denatured homogenates is consistent with a specific protein conformation-dependent recognition of NAB-daunorubicin beyond that which would be expected from random low affinity interaction with native or denatured proteins. In addition, when the lipid components of the photolabeled heart homogenates were extracted with chloroform:methanol (2:1, v/v), no radioactive macromolecular components (>10 kDa) were found in the organic layer.

Characterization of heart homogenate photolabeling. When heart homogenate was incubated with ^{3}H-NAB-daunorubicin in the absence of UV light for 30 min, no radioactivity above ambient background was found in SDS-PAGE gel slices except for excess ^{3}H-NAB-daunorubicin which migrated near the tracking dye front. Similar results were obtained after photoactivating ^{3}H-NAB-daunorubicin in the absence of heart homogenate and then immediately adding the heart homogenate and performing the SDS-PAGE. Maximum photolabeling of 18.3- and 31.2-kDa polypeptides was seen within 10–12 min of UV irradiation over a wide range (0.06–0.6 μM) of initial ^{3}H-NAB-daunorubicin concentrations and was linear up to at least 150 μg of heart homogenate protein.

The photolabeling of heart homogenate in the presence of the nitrene-reactive scavengers, *p*-aminobenzoate and β-mercaptoethanol, did not have a significant effect on 18.3- or 31.2-kDa polypeptide radiolabeling at a 10^3-fold molar excess of scavenger over ^{3}H-NAB-daunorubicin. In fact, no significant reduction in photolabeling was observed unless scavengers were present in a 10^4-fold molar excess. The absence of a significant effect on photolabeling by 10^3-fold molar excess of nitrene scavengers confirms that labeling occurs by a true photoaffinity mechanism rather than by a pseudo-photoaffinity mechanism (23, 24).

Anthracycline photolabeling specificity of rat heart 18.3-kDa polypeptide. In the presence of increasing concentrations of ^{3}H-NAB-daunorubicin, photolabeling of 18.3-kDa polypeptide reached an apparent saturable maximum of 2.42 ± 0.47 pmol of ^{3}H-NAB-daunorubicin bound/mg of heart homogenate protein. By reciprocal analysis, half-maximal photolabeling was achieved at 36 nM ^{3}H-NAB-daunorubicin (Fig. 5). Furthermore, a 16-fold molar excess of nonradioactive analogue reduced photolabeling by 90%. In contrast, a linear increase in the photolabeling of 31.2-kDa polypeptide and in the average baseline radioactivity was observed up to 0.62 μM ^{3}H-NAB-daunorubicin (Fig. 5). In the presence of a 16-fold molar excess

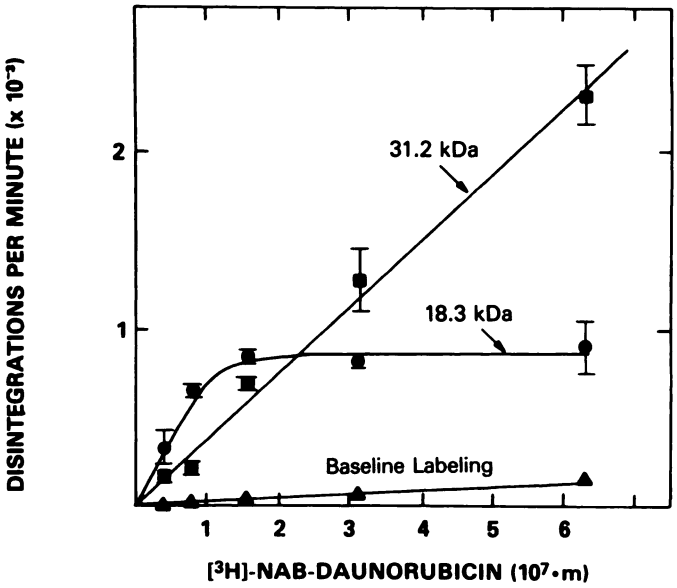

Fig. 5. Photolabeling of 38 μg of rat heart homogenate protein with increasing concentrations of ^{3}H-NAB-daunorubicin (5.06 Ci/mmol). Each *point* represents the mean integrated radioactivity (n = 3) minus average baseline radioactivity ± standard deviation of the indicated labeled components: ●, 18.3 kDa; ■, 31.2 kDa; and △, baseline radioactivity minus the ambient background.

of nonradioactive analogue, 31.2-kDa radiolabeling was reduced only 25% and the baseline radiolabeling was unaffected.

We established the 18.3-kDa and 31.2-kDa polypeptide photolabeling requirement for the daunomycinone ring by comparing the ^{3}H-NAB-daunorubicin photolabeling pattern of heart homogenates to the patterns obtained with the photoactive model compounds ^{3}H-NAB-daunosamine and ^{3}H-NAB-ethanolamine. In contrast to the extensive photolabeling of 18.3- and 31.2-kDa polypeptides by ^{3}H-NAB-daunorubicin, the model compounds ^{3}H-NAB-daunosamine and ^{3}H-NAB-ethanolamine, both lacking the daunomycinone ring, weakly photolabeled only a 14.6-kDa species (data not shown). The 14.6-kDa component was confirmed as being electrophoretically distinct from the 18.3-kDa component by mixing heart homogenates which had been separately photolabeled with either ^{3}H-NAB-daunorubicin or ^{3}H-NAB-ethanolamine and coelectrophoresing them in the same SDS-PAGE lane.

The 18.3- and 31.2-kDa polypeptide photolabeling dependence on the daunomycinone ring was further analyzed by comparing radiolabeling profiles obtained by photolabeling heart homogenate with ^{3}H-NAB-daunorubicin, ^{3}H-NAB-Adriamycin or ^{3}H-NAB-carminomycin (Table 1). The 31.2-kDa polypeptide was photolabeled to the same extent by all three anthracycline analogues. In contrast, 18.3-kDa polypeptide photolabeling with NAB-Adriamycin was dramatically reduced, whereas photolabeling with NAB-carminomycin was negligible. These results demonstrate the molecular structural dependence on the anthracyclinone ring for the photolabeling of the 31.2- and 18.3-kDa polypeptides. However, whereas 31.2-kDa polypeptide photolabeling was insensitive to changes in anthracyclinone ring functional side chains, maximum photolabeling of 18.3-kDa polypeptide by NAB-daunorubicin confirmed its preference for the daunomycinone ring.

The effect of daunorubicin amino sugar *N*-substitution on photolabeling was studied by labeling heart homogenates with

TABLE 1

Relative photolabeling of rat heart 18.5- and 31.2-kDa polypeptides with ^{3}H-NAB-daunorubicin, ^{3}H-NAB-Adriamycin, and ^{3}H-NAB-carminomycin

Drug Analogue	Radiolabeled polypeptides[a]		Ratio[b]
	18.5 kDa	31.2 kDa	
	pmol/mg protein		
^{3}H-NAB-daunorubicin	1.21 ± 0.257	0.483 ± 0.097	2.5
^{3}H-NAB-Adriamycin	0.595 ± 0.118 ($p < 0.02$)[c]	0.544 ± 0.017 ($p > 0.5$)	0.914
^{3}H-NAB-carminomycin	0.022 ± 0.014 ($p < 0.01$)	0.380 ± 0.046 ($p > 0.1$)	0.058

[a] Values are means ± standard deviations ($n = 3$).
[b] pmol of 18.3-kDa polypeptide/pmol of 31.2-kDa polypeptide.
[c] Statistical comparison of photolabeling of polypeptides to the same polypeptide photolabeled with ^{3}H-NAB-daunorubicin was by the Student's t test.

^{3}H-NAB-daunorubicin in the presence of increasing concentrations of nonphotoactive daunorubicin analogues. The presence of *N*-substituted daunorubicin competitors significantly reduced specific photolabeling without affecting the baseline radioactivity. For example, a 10-fold molar excess of *N*-(*p*-aminobenzoyl)-daunorubicin reduced 18.3- and 31.2-kDa polypeptide photolabeling by 35% and 23%, respectively (Fig. 6A). Furthermore, when the inhibition data from Fig. 6A were analyzed as originally suggested by Ofengand and Henes (49) and recently applied to photolabeling experiments (50), the resultant linear replots confirmed that the ^{3}H-NAB-daunorubicin and the competitor interacted with the same binding site (Fig. 6B). When the slope of the 18.3-kDa replot in Fig. 6B was used to estimate the K_D of the competitor relative to that of ^{3}H-NAB-daunorubicin, the K_D of the 18.3-kDa polypeptide for *N*-(*p*-aminobenzoyl)-daunorubicin was calculated to be 25 times that of the K_D for ^{3}H-NAB-daunorubicin. Similar photolabeling experiments carried out in the presence of *N,N'*-dibenzyldaunorubicin, *N*-acetyldaunorubicin, or unsubstituted daunorubicin gave K_D values relative to that of ^{3}H-NAB-daunorubicin of 100, 330, and 1500, respectively. As expected, the closest structural analogue of NAB-daunorubicin tested, *N*-(*p*-aminobenzoyl)-daunorubicin, also was the most effective binding inhibitor. These results demonstrate that all of the anthracycline analogues tested have high affinities for the 18.3-kDa polypeptide.

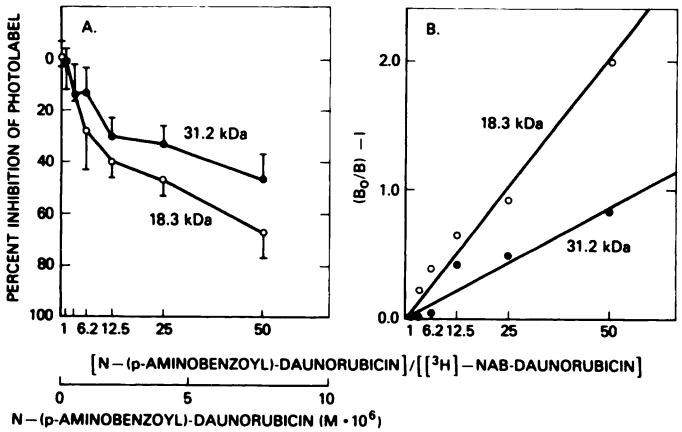

Fig. 6. Photolabeling of rat heart homogenate (38 μg of protein) with 0.16 mM ^{3}H-NAB-daunorubicin (10.12 Ci/mmol) in the presence of increasing concentrations of *N*-(*p*-aminobenzoyl)-daunorubicin. B, Replot of the data from A according to the equation $(B_o/B)-1 = K_r$ [*N*-(*p*-aminobenzoyl)-daunorubicin]/[^{3}H-NAB-daunorubicin], where B_o and B are the incorporation of radioactivity into 18.3-kDa or 31.2-kDa polypeptides in the absence and presence of *N*-(*p*-aminobenzoyl)-daunorubicin, respectively, and K_r is the ratio of K_D of *N*-(*p*-aminobenzoyl)-daunorubicin to K_D of NAB-daunorubicin.

***In vitro* NAB-daunorubicin metabolism.** Identical radioactive profiles were obtained after preincubating ^{3}H-NAB-daunorubicin with heart homogenates for 1, 30, or 60 min followed by photolabeling at 25° for 10 min. The same relative patterns resulted when preincubation and photolabeling were carried out at 0° or 37°. These results suggested that, under these photolabeling conditions, *in vitro* metabolism did not occur or, if it did occur, the basic NAB-daunorubicin structure-dependent labeling was not altered. These two possibilities were further evaluated by incubating NAB-daunorubicin or ^{3}H-NAB-daunorubicin with heart homogenates under conditions approximating the standard photolabeling conditions and analyzing for fluorescent or radioactive metabolites by HPLC or silica gel TLC, respectively. After a 60-min incubation, no fluorescent metabolites were detected. In addition, >90% of the total radioactivity detected on TLC was accounted for by ^{3}H-NAB-daunorubicin with only 1.5–2.9% corresponding to NAB-daunorubicinol and 3.2–3.3% corresponding to NAB-daunosamine. Thus, under conditions used in our photolabeling experiments, little or no metabolism was found. This precluded a significant metabolic effect on the specificity of NAB-daunorubicin photolabeling.

Discussion

The identification of anthracycline-binding polypeptides by photoaffinity labeling is based on the assumption that a reversible complex occurs between the photoactive anthracycline analogue and polypeptide acceptor sites which specifically recognize structural characteristics of the drug. Irradiation then converts the analogue into a reactive nitrene intermediate which will covalently attach at or near the acceptor-binding sites (23, 24). Since the nitrene intermediate has a short half-life reactivity, the photoactivated anthracycline analogue should efficiently label only those acceptors to which it is closely associated. Thus, photoaffinity labeling should identify those cellular components with the highest affinity for anthracycline antibiotics, and a significant relationship may be established between those most prominently labeled acceptors and the biochemical or pharmacological activities of the photoactive anthracycline analogue, in particular, or of anthracycline antibiotics, in general.

Anthracycline antibiotic macromolecular interactions were identified in several rat tissues by photolabeling with the photoactive anthracycline analogue, ^{3}H-NAB-daunorubicin. Primary attention was directed toward the 18.3- and 31.2-kDa polypeptides which were the most prominently labeled species

in heart homogenate as well as in all other tissues examined. Subsequent characterization of these labeled polypeptides confirmed that the 18.3-kDa acceptor fulfilled all of the basic criteria assumed for the identification of a specific anthracycline-binding acceptor using photoaffinity labeling. In comparison, the properties of the 31.2-kDa polypeptide reflected a more general anthracycline antibiotic association.

Perhaps the most significant property of the 18.3-kDa acceptor is its saturable photolabeling. Saturable photolabeling is consistent with the formation of a reversible binary complex between NAB-daunorubicin and the 18.3-kDa polypeptide prior to photoactivation. Saturation was not the result of incomplete photolabeling due to absorption of UV activation light by excess photoactive analogue, because identical photoactivation kinetics were obtained over a wide NAB-daunorubicin concentration range. The possibility that a concentration-dependent self-polymerization of the photoactive analogue might explain the saturation was excluded by the observation that the simultaneous photolabeling of 31.2-kDa polypeptide remained nonsaturable up to 0.62 μM NAB-daunorubicin.

Because photolabeling was less than 100% efficient, it was not possible to determine the true equilibrium constant for binary complex formation. However, with a half-maximal saturation photolabeling concentration of 36 nM, the saturable photolabeling data also were consistent with a high affinity recognition by the 18.3-kDa acceptor of the photoactive analogue.

The photoaffinity labeling of anthracycline-binding polypeptides was dependent on the recognition of the major anthracycline antibiotic structural features by the acceptor. These unique structural characteristics were identified by photolabeling heart homogenates with several different photoactive anthracycline analogues and model compounds. The results showed that both the 18.3-kDa and the 31.2-kDa polypeptides exhibited an absolute photolabeling dependency on the anthracyclinone ring. However, whereas 31.2-kDa polypeptide was photolabeled equally well with several anthracycline analogues, each having a different anthracyclinone ring, the 18.3-kDa polypeptide exhibited an optimum photolabeling dependency for the daunomycinone ring.

The importance of anthracycline antibiotic structure to photolabeling also was studied by competitive inhibition of NAB-daunorubicin photolabeling by different anthracycline analogues. The results revealed that the 18.3-kDa polypeptide exhibits highest affinity for the *N*-substituted antibiotic sugars. Nevertheless, this polypeptide also has high affinity for unsubstituted daunorubicin. *In toto*, the results suggest that amino sugar *N*-substitution contributes to the overall NAB-daunorubicin photolabeling specificity of 18.3-kDa polypeptide, but that it augments the basic daunomycinone ring specificity and is not sufficient by itself to direct the photolabeling of the 18.3-kDa polypeptide.

The localization of the 18.3-kDa and 31.2-kDa polypeptides to the inner mitochondrial membrane may be a clue to the identification of their biochemical function(s). For example, anthracycline antibiotics inhibit oxidative phosphorylation in cells and isolated mitochondria (3). Evidence suggests a specific interaction of anthracyclines with the mitochondrial ubiquinone-mediated electron transport enzymes (51, 52). Interestingly, ubiquinone-binding proteins of 17 kDa and 37 (or 30) kDa have been identified in beef heart mitochondria by photoaffinity labeling with arylazide and azidoubiquinone derivatives (53, 54). The anthracycline-binding polypeptides identified in this study are remarkably similar in size to these ubiquinone acceptors. Furthermore, the greater anthracyclinone ring specificity of the 18.3-kDa acceptor relative to that of the 31.2-kDa acceptor is directly analogous to the greater specificity of the 17-kDa protein for ubiquinone compared to that of the 37 (or 30)-kDa protein (54).

The presence of specific anthracycline-binding polypeptides in heart plus their possible involvement with ubiquinone-related electron transport suggests there may be a role for 18.3-kDa and/or 31.2-kDa acceptors in the mechanism of anthracycline antibiotic-induced cardiotoxicity (27). It appears that mitochondrial complex I is capable of producing anthracycline semiquinone free radicals and reactive oxygen metabolites which mediate the subcellular organelle and membrane disintegration associated with anthracycline cardiotoxicity (55, 56). If the 18.3-kDa and/or 31.2-kDa polypeptides normally function as ubiquinone-binding components of complex I, then their affinity to anthracycline antibiotics might facilitate a single electron reduction of the drug to the semiquinone free radical. In light of recent reports that the anthracycline analogue, carminomycin, is less cardiotoxic (57), photolabeling of the 18.3-kDa polypeptide with photoactive daunorubicin and adriamycin analogues but not by a photoactive carminomycin analogue supports the suggested involvement of this acceptor in the cardiotoxic mechanism of anthracycline antibiotics.

We have also identified an analogous 18.3-kDa anthracycline-binding polypeptide in several tumor cell lines *in vitro*.[3] The presence of variable amounts of this anthracycline acceptor in drug-sensitive and drug-resistant murine leukemic cells suggests that it could play a role in the antitumor activity of anthracycline antibiotics in these cells.

Numerous anthracycline antibiotic analogues have been synthesized and tested for their potential antineoplastic activity (58). The substitution of a proton of the free amino group of class I anthracyclines with various groups has yielded compounds having chemical properties and pharmacological activities which differ from that of the parent drug. One of the most consistent differences is reduced interaction of *N*-substituted analogues with double-stranded DNA (59, 60). Consequently, N-substituted drugs exhibit a weaker inhibition of nucleic acid synthesis and in some cases are localized primarily to the cytoplasm (2, 26). These and other properties have stimulated a search for alternative or additional mechanisms of actions and have revealed the interaction of anthracyclines with subcellular organelles such as plasma membrane, mitochondria, and lysosomes, and with cellular proteins, lipids, and polysaccharides (1–21). In addition, their effects on various cellular activities have led to a number of suggested functions that differ from the traditional involvement of anthracyclines in nuclear-associated events. Our data illustrate the utility of photoaffinity labeling to probe for specific anthracycline antibiotic cellular acceptors which may be mediators of anthracycline antibiotic function. We are currently using NAB-daunorubicin as well as photoactive analogues of vinblastine to identify common cellular targets which might be involved in the mechanism of pleiotropic drug resistance[4] (61).

[3] Unpublished data.
[4] Unpublished data.

Considering the close homology of the photoactive anthracycline analogue to other *N*-substituted anthracyclines, we predict that NAB-daunorubicin will be useful for identifying cytoplasmic targets which mediate the biochemical actions of this class of drugs. An additional benefit is the significant binding of NAB-daunorubicin by cellular acceptors that recognize the anthracyclinone ring. Consequently, NAB-daunorubicin is an important probe for general as well as specific anthracycline-binding sites and will be useful for characterizing previously identified as well as novel pathways of anthracycline antibiotic action.

Acknowledgments

The authors would like to thank Drs. Nicholas R. Bachur and Ahmad R. Safa for helpful and encouraging advice, Dr. James Kelley, Dr. John Strong, and Mr. Larry Anderson for performing the mass spectroscopy, Nancy Malinowski and Jenny Sewell for their excellent technical assistance, and Beverly Sisco for the preparation of this manuscript.

References

1. Peterson, C., and A. Trouet. Transport and storage of daunorubicin and doxorubicin in cultured fibroblasts. *Cancer Res.* **38**:4645–4649 (1978).
2. Egorin, M. D., R. E. Clawson, J. I. Cohen, L. A. Ross, and N. R. Bachur. Cytofluorescence localization of anthracycline antibiotics. *Cancer Res.* **40**:4669–4676 (1980).
3. Muhammed, H., G. Ramasarma, and C. K. R. Kurup. Inhibition of mitochondrial oxidative phosphorylation by adriamycin. *Biochim. Biophys. Acta* **722**:43–50 (1982).
4. Tritton, T. R., and G. Yee. The anticancer agent adriamycin can be actively cytotoxic without entering cells. *Science (Wash D. C.)* **217**:248–250 (1982).
5. Zenebergh, A., P. Baurain, and C Trouet. Cellular pharmacokinetics of aclacinomycin A in cultured L1210 cells. *Cancer Chemother. Pharmacol.* **8**:243–249 (1982).
6. Broggini, M., P. Ghersa, and M. G. Donelli. Subcellular distribution of adriamycin in the liver and tumor of 3LL-bearing mice. *Eur. J. Clin. Oncol.* **19**:419–426 (1983).
7. Robers, K. E., B. I. Carr, and Z. A. Tökés. Cell surface-mediated cytoxicity of polymer-bound adriamycin against drug-resistant hepatocytes. *Cancer Res.* **43**:2741–2748 (1983).
8. Zunino, T., R. Gambetta, A. Di Marco, and A. Zaccara. Interaction of daunomycin and its derivatives with DNA. *Biochim. Biophys. Acta* **177**:489–498 (1972).
9. Duarte-Karim, M., J. M. Ruysschaet, and I. Hildebrand. Affinity of adriamycin to phospholipids; a possible explanation for cardiac mitochondrial lesions. *Biochem. Biophys. Res. Commun.* **71**:658–663 (1976).
10. Kikuchi, H., and S. Sato. Binding of daunomycin to nonhistone proteins from rat liver. *Biochim. Biophys. Acta* **434**:509–512 (1976).
11. Na, C., and S. N. Timasheff. Physical-chemical study of daunomycin-tubulin interactions. *Arch. Biochem. Biophys.* **182**:147–154 (1977).
12. Goldman, R., T. Focchinetti, D. Boch, A. Raz, and M. Shinitzky. A differential interaction of daunomycin, adriamycin and their derivatives with human erythrocytes and phospholipid bilayers. *Biochem. Biophys. Acta* **512**:254–269 (1978).
13. Menozzi, M., and T. Arcamone. Binding of adriamycin to sulphated mucopolysaccharides. *Biochem. Biophys. Res. Commun.* **80**:313–318 (1978).
14. Mikkelsen, R. B., P. S. Lin, and D. F. H. Wallach. Interaction of adriamycin with human red blood cells: a biochemical and morphological study. *J. Mol. Med.* **2**:33–39 (1977).
15. Someya, A., T. Akiyama, M. Misumi, and N. Tanaka. Interaction of anthracycline antibiotics with actin and heavy meromyosin. *Biochem. Biophys. Res. Commun.* **85**:1542–1550 (1978).
16. Taylor, R. F., L. A. Teague, and D. W. Yesair. Drug-binding macromolecular lipids from L1210 leukemia tumors. *Cancer Res.* **41**:4316–4323 (1981).
17. Eksborg, S., H. Ehrsson, and B. Ekquist. Protein binding of anthraquinone glycosides with special reference to Adriamycin. *Cancer Chemother. Pharmacol.* **10**:7–10 (1982).
18. Fisher, J., K. Ramakrishnan, and K. E. McLane. Complexation of anthracycline antibiotics by the apo egg white riboflavin binding protein. *Biochemistry* **21**:6172–6180 (1982).
19. Lewis, W., J. Kleinerman, and S. Puszkin. Interaction of adriamycin *in vitro* with cardiac myofibrillar proteins. *Circulation Res* **50**:547–553 (1982).
20. Fisher, J., K. Ramakrishnan, and J. E. Becvar. Direct enzyme-catalyzed reduction of anthracyclines by reduced nicotinamide adenine dinucleotide. *Biochemistry* **22**:1347–1355 (1983).
21. Gambetta, R. A., O. Colombo, C. Lanzi, and T. Zunino. Purification and partial characterization of a daunorubicin-binding protein from rat liver. *Mol. Pharmacol.* **24**:336–340 (1983).
22. Pan, S. S., L. Pedersen, and N. R. Bachur. Comparative flavoprotein catalyses of anthracycline antibiotics. *Mol. Pharmacol.* **19**:184–186 (1981).
23. Chowdhry, V., and F. H. Westheimer. Photoaffinity labeling of biological systems. *Annu. Rev. Biochem.* **48**:293–325 (1979).
24. Fedan, J. S., G. K. Hogaboom, and J. P. O'Donnell. Photoaffinity labels as pharmacological tools. *Biochem. Pharmacol.* **33**:1167–1180 (1984).
25. Yee, G., M. Carey, and T. R. Tritton. Photoaffinity labeling of the sarcoma 180 cell surface by daunomycin. *Cancer Res.* **44**:1898–1903 (1984).
26. Averbuch, S. D., R. E. Clawson, N. R. Bachur, and R. L. Felsted. Cellular phramacology and antitumor activity of *n*-(*p*-azidobenzoyl) daunorubicin, a photoactive anthracycline analogue. *Cancer Chemother. Pharmacol.* **16**:211–217 (1986).
27. Ferrans, V. J. Overview of cardiac pathology in relation to anthracycline cardiotoxicity. *Cancer Treat. Rep.* **62**:955–961 (1978).
28. Bachur, N. R., and M. Gee. Daunorubicin metabolism by rat tissue preparations. *J. Pharmacol. Exp. Ther.* **177**:567–571 (1971).
29. Felsted, R. L., M. Gee, and N. R. Bachur. Rat liver daunorubicin reductase, an aldo-keto reductase. *J. Biol. Chem.* **249**:3672–3679 (1974).
30. Staros, J. V., H. Bayley, D. N. Standring, and J. R. Knowles. Reduction of aryle azides by thiols: implications for the use of photoaffinity reagents. *Biochem. Biophys. Res. Commun.* **80**:568–572 (1978).
31. Mela, T., and S. Seitz. Isolation of mitochondria with emphasis on heart mitochondria from small amounts of tissue. *Methods Enzymol.* **55**:39–46 (1979).
32. Idell-Wenger, J. A., L. W. Grotyohann, and J. R. Neely. An improved method for isolation of mitochondria in high yields from normal, ischemic and autolyzed rat hearts. *Anal. Biochem.* **125**:269–276 (1982).
33. Palmer, J. W., B. Tandler, and C. L. Hoppel. Biochemical properties of subsarcolemmal and interfibrillar mitochondria isolated from rat cardiac muscle. *J. Biol. Chem.* **252**:8731–8739 (1977).
34. Schaitman, V. C., V. G. Erwin, and J. W. Greenwalt. The submitochondrial localization of monoamine oxidase: an enzymatic marker from the outer membrane of rat liver mitochondria. *J. Cell Biol.* **32**:719–735 (1967).
35. Sottocasa, G. L., B. Kuylenstierna, L. Ernster, and A. Berstrand. An electron-transport system associated with the outer membrane of liver mitochondria. A biochemical and morphological study. *J. Cell Biol.* **32**:415–438 (1967).
36. Sellinger, O. Z., H. Beaufay, P. Jacques, A. Doyen, and C. de Duve. Intracellular distribution and properties of β-*N*-acetylglucosaminidase and β-galactosidase in rat liver. *Biochem. J.* **74**:450–456 (1960).
37. Ipata, P. L. A coupled optical enzyme assay for 5′-nucleotidase. *Anal. Biochem.* **20**:30–36 (1967).
38. Vailee, R. B. The two-stage reversible denaturation of lactate dehydrogenase at low pH in isoenzymes. in *Mol. Struct. J.* **1**:151–167 (1975).
39. Sorbahl, L. A., C. Johnson, Z. R. Blailock, and A. Schwartz. The mitochondrion. *Methods Pharmacol.* **1**:247–286 (1971).
40. Pedersen, P. L., J. W. Greenawalt, B. Reynafarze, J. Hullihen, G. L. Decker, O. W. Supes, and E. Buftamente. Preparation and characterization of mitochondria and submitochondrial particles of rat liver and liver derived tissues. *Methods Cell Biol.* **20**:411–481 (1978).
41. Goridis, C., and N. H. Neff. Monoamine oxidase: an approximation of turnover rates. *J. Neurochem.* **18**:1673–1682 (1971).
42. Sottocasa, G. L., B. Kuylenstierna, L. Ernster, and A. Bergstrand. Separation and some properties of the inner and outer membranes of rat liver mitochondria. *Methods Enzymol.* **10**:448–463 (1979).
43. Beaufay, H. and A. Amar-Costesec. Cell fractionation techniques. *Methods Membr. Biol.* **6**:1–100 (1976).
44. Laemmli, U. K. Cleavage of structural proteins during the assembly of the head of bacteriophage T_4. *Nature (Lond.)* **227**:680–685 (1970).
45. Andrews, P. A., D. E. Brenner, F. T. E. Chow, H. Kubo, and N. R. Bachur. Facile and definitive determinations of human adriamycin and daunorubicin metabolites by high-pressure liquid chromatography. *Drug Metab. Dispos.* **8**:152–156 (1980).
46. Lowry, O. H., N. J. Rosebrough, A. L. Farr, and R. J. Randall. Protein measurement with the Folin phenol reagent. *J. Biol. Chem.* **193**:265–275 (1951).
47. Bonner, W. M., and R. Laskey. A film detection method for tritium-labelled proteins and nucleic acids in polyacrylamide gels. *Eur. J. Biochem.* **46**:83–88 (1974).
48. Williams, B. A., and T. R. Tritton. Photoactivation of anthracyclines. *Photochem. Photobiol.* **34**:131–134 (1981).
49. Ofengand, J., and C. Henes. The function of pseudouridylic acid in transfer ribonucleic acid. *J. Biol. Chem.* **244**:6241–6253 (1969).
50. Gehlen, R. L., and B. E. Haley. Use of a GTP photoaffinity probe to resolve aspects of the mechanism of tubulin polymerization. *J. Biol. Chem.* **254**:11982–11987 (1979).
51. Iwamoto, Y., I. T. Hansen, T. H. Porter, and K. Folkers. Inhibition of coenzyme Q_{10}-enzymes, succinoxidase and NADH-oxidase by adriamycin and other quinones having antitumor activity. *Biochem. Biophys. Res. Commun.* **58**:633–638 (1974).
52. Kishi, T., T. Watanabe, and K. Folkers. Bioenergetics in clinical medicine: prevention by forms of coenzyme Q of the inhibition by adriamycin of coenzyme Q_{10}-enzymes in mitochondria of the myocardium. *Proc. Natl. Acad. Sci. USA* **73**:4653–4656 (1976).
53. Yu, T., and C. A. Yu. The interaction of arylzido-ubiquinone derivative with mitochondrial ubiquinol-cytochrome *c* reductase. *J. Biol. Chem.* **257**:10215–10221 (1982).

54. Yu, T., T. D. Yand, and C. A. Yu. Interaction and identification of ubiquinone-binding proteins in ubiquinone-cytochrome *c* reductase by azido-ubiquinone derivatives. *J. Biol. Chem.* **260**:963–973 (1985).
55. Doroshow, J. H. Anthracycline antibiotic-stimulated superoxide, hydrogen peroxide, and hydroxyl radical production by NADH dehydrogenase. *Cancer Res.* **43**:4543–4551 (1983).
56. Doroshow, J. H. Effect of anthracycline antibiotics on oxygen radical formation in heart. *Cancer Res.* **43**: 460–472 (1983).
57. Crooke, S. T. A review of carminomycin—a new anthracycline developed in the U.S.S.R. *J. Med. (Westbury)* **8**:293–311 (1977).
58. Arcamone, T. Properties of antitumor anthracyclines and new developments in their application: Cain Memorial Award Lecture. *Cancer Res.* **45**:5995–5999 (1985).
59. Sengupta, S. H., R. Seshadri, E. J. Modest, and M. Israel. Comparative DNA-binding studies with adriamycin (ADR), *N*-trifluoracetyl-adriamycin-14-valerate (AD 32) and related compounds. *Proc. Am. Assoc. Cancer Res.* **17**:109 (1976).
60. Traganos, F., M. Israel, R. Silber, S. Seshadri, S. Kirchenbaum, and M. Potmesil. Effects of new *N*-alkyl analogues of adriamycin on *in vitro* survival and cell cycle progression of L1210 cells. *Cancer Res.* **45**:6273–6279 (1985).
61. Safa, A. R., C. J. Glover, M. B. Meyers, J. L. Biedler, and R. L. Felsted. Vinblastine photoaffinity labeling of a high molecular weight surface membrane glycoprotein specific for multidrug-resistant cells. *J. Biol. Chem.* **261**:6137–6140 (1986).

Send reprint requests to: Dr. Ronald L. Felsted, Laboratory of Biological Chemistry, Developmental Therapeutics Program, Division of Cancer Treatment, National Cancer Institute, National Institutes of Health, Building 37, Room 5D02, Bethesda, MD 20892.